Continuous co-crystallisation of Carbamazepine and Trans-Cinnamic acid via melt extrusion processing

ARTICLE *in* CRYSTENGCOMM · FEBRUARY 2014

Impact Factor: 4.03 · DOI: 10.1039/C3CE42457J

CRYSTAL GROWTH & DESIGN

Article

pubs.acs.org/crystal

Continuous Cocrystallization for Dissolution Rate Optimization of a Poorly Water-Soluble Drug

Hiren Moradiya,[†] Muhammad T. Islam,[†] Grahame R. Woollam,[‡] Ian J. Slipper,[†] Sheelagh Halsey,[§] Martin J. Snowden,[†] and D. Douroumis*[,†]

[†] Faculty of Engineering and Science, University of Greenwich, Chatham Maritime, Chatham, ME4 4TB, Kent, U.K.

[‡]Novartis Pharma AG, Werk Klybeck, Klybeckstrasse 141, CH-4057 Basel, Switzerland

[§]Molecular Spectroscopy and Material Characterization, Thermo Fisher Scientific, Hemel Hempstead, HP2 7GE, U.K.

Supporting Information

ABSTRACT: A continuous manufacturing process, hot melt extrusion (HME), was employed for the development of high quality carbamazepine−saccharin (CBZ−SCH) cocrystals. The produced cocrystals were compared with a prototype prepared by a solvent method. It was found that processing parameters such as temperature, screw speed, and screw configuration were the critical processing parameters. In-line near-infrared analysis demonstrated that cocrystallization takes place gradually during the process along the extruder's mixing zones. Further characterization of the extruded cocrystals proved that the manufactured highly crystalline cocrystals were similar to the prototype but had improved CBZ dissolution rates. Continuous manufacturing of cocrystals of water-insoluble drugs is a novel and robust approach.

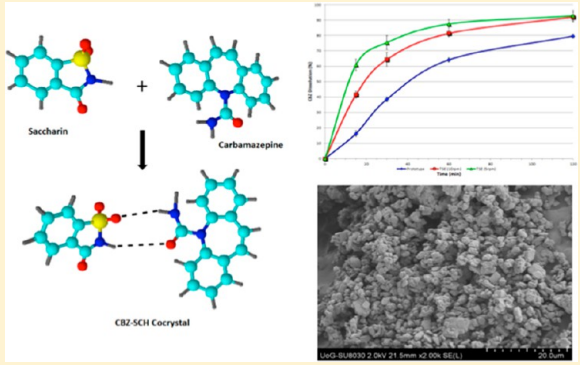

INTRODUCTION

The oral route of drug administration is most preferable because it is convenient, inexpensive, patient friendly, and easier to administer than other routes. However, with poorly water-soluble drugs, that is, class II drugs in the Biopharmaceutics Classification System (BCS), traditional formulation can lead to low bioavailability of the drug. Around 60% of drugs that are screened during industrial research are poorly water-soluble.[1] Therefore, the enhancement of poorly soluble drugs is becoming increasingly important in industry and research.

Cocrystallization is a novel approach to engineer the bulk properties of poorly soluble active pharmaceutical ingredients (APIs) where it can switch the molecular interactions between components and result in unique structure composition.[2−6] This modification provides superior solubility and stability, better release, and thus better bioavailability[7] for the molecule without affecting its physiological action.[8,9] Further studies also noted that the multilayered structure of cocrystals improved mechanical properties and gave better flow properties and compressibility, which could be helpful in dosage form preparation.[10,11] Pharmaceutical cocrystals are normally formed between an API and an accepted coformer, which should not interact with the drug entity to produce an unacceptable product. The cocrystals can be defined as crystalline complexes of two or more neutral molecular constituents bound through noncovalent interactions within the crystal lattice.[12,13] It has been proven that cocrystal solubility is directly proportional to the solubility of the constituent reactant but also to the concentration of the coformer.[7]

Conventionally, a cocrystal is developed by a solvent method or particle size reduction by grinding. Solvent methods include slurry conversion, solvent evaporation, cooling crystallization, and precipitation. The grinding method involves grinding of two or more components by hand or mill.[14] Grinding is carried out with a small amount of solvent when the grinding method needs a catalyst. However, scale up of these conventional methods is a major challenge. Recently, thermal inkjetting was reported as an alternative approach for the manufacturing of cocrystals, where the coformers were dissolved in water or water−ethanol solutions.[15] The use of toxic solvents during processing is an additional burden to overcome because it is a costly process and requires a special disposal system. Utilization of solvents also has potential health and environmental effects (e.g., air pollution). In addition, with solvent methods, equal solubility is required for the dissolved components in order to avoid precipitation in the solution.

Hot melt extrusion (HME) is a novel technique adapted from the plastic and polymer industries. Growing attention can be seen in HME as it is widely utilized for various pharmaceutical applications. Hot melt extrusion is a continuous process that draws materials toward a die with a constant screw speed and

Received: September 15, 2013
Revised: November 14, 2013
Published: November 22, 2013

elevated temperature to get uniformly shaped pellets or strips.[16] Some major advantages of HME are as follows: it is a continuous process, it is easy to scale up, and quality assurance can be monitored by PAT (process analytical technology). High friction takes place between the barrel and the screws at the desired temperature inducing excellent mixing of solid materials. In addition, HME is considered a green technology because processing of materials does not require the usage of organic solvents.

Previously Dhumal et al.[17] reported cocrystallization of ibuprofen with nicotinamide with hot melt extrusion. They described the processing temperature and the screw configuration as key variables in HME to obtain cocrystals. Similarly, Daurio et al.[18] presented HME as an effective method for making cocrystals and applied liquid assisted extrusion for cocrystallization.

In this work, carbamazepine (CBZ), a Class 2 BCS active, was used with saccharin (SCH) as a coformer. Carbamazepine is a widely used anticonvulsant drug having poor aqueous solubility and high permeability. HME was employed to produce CBZ and SCH cocrystals by investigating processing parameters. The cocrystals produced were compared with prototype cocrystals developed by a solvent method.[19]

EXPERIMENTAL SECTION

Materials. Carbamazepine (CBZ, 98%) and saccharin (SCH, purity >99%) were purchased from Sigma-Aldrich (Gillingham, UK) and used without any further treatment. All solvents used for HPLC were analytical grade.

Hot Melt Extrusion Continuous Manufacturing. Carbamazepine and saccharin, 1:1 molar ratio, were weighed accurately and blended to uniformity in a turbula mixer for 10 min. The powder blends were extruded using a single screw extruder (Randcastle, US) and a corotating twin screw extruder (Eurolab-16, Thermo Fisher, Germany) with two different screw speeds, 5 and 10 rpm. Extrusion was carried out without a die. Typical temperature profiles used within different zones of the extruder from hopper to extruder were 70 °C, 95 °C, 110 °C, 120 °C, 120 °C, 120 °C, 120 °C, 115 °C. However, the maximum temperature was adjusted in order to optimize the cocrystal quality and was varied from 120 to 140 °C.

Cooling Cocrystallization Process. CBZ−SCH cocrystals were prepared according to Hickey et al.[19] Briefly, the solids were dissolved in 280 mL of a 62.5/37.5% v/v ethanol/methanol (both from EM Science) and heated to 70 °C for 1 h under reflux. The temperature was decreased in 10 °C increments to induce precipitation in a stirred, unseeded system. Appearance of the cocrystal solid phase was first observed in the range of 60−50 °C. The temperature was further lowered to 30 °C to drive additional precipitation. Following equilibration at 30 °C, the solids were isolated using a Buchner funnel and rinsed with cold ethanol.

Differential Scanning Calorimetry (DSC). The thermal behavior of bulk CBZ, the physical mixture (PM) of CBZ−SCH, the prototype, and extruded cocrystals were examined by employing a differential scanning calorimeter (Mettler Toledo 823e, Greifensee, Switzerland). Accurately weighed, 3−5 mg samples were placed into an aluminum pan, which was crimped. Each pan was heated from 0 to 200 °C at 10 °C/min heating rate, and the flow rate of nitrogen gas was 20 mL/min. Star evaluation software was used for analysis of the data.

Hot Stage Microscopy (HSM). The hot stage microscopy experiments were conducted on a Mettler Toledo FP82HT (Greifensee, Switzerland) with a Nikon Microphot SA. Powder cocrystals were sprinkled on a glass slide, covered with a coverslip, and heated from ambient room temperature to 220 °C at 10 °C per minute. Changes in morphology behavior were collected as a video recording by using PixeLINK PL-A662 camera (PixeLINK, Ontario, US).

Powder X-ray Diffraction. Data were collected on a D8 Advance X-ray diffractometer (Bruker, Germany) in $\theta-\theta$ geometry using both reflection and foil transmission modes. A Cu anode X-ray tube was powered at 40 kV and 40 mA. We used a primary Göbel mirror for parallel beam and removal of Cu Kβ, a primary 4° Soller slit, a secondary 2.5° Soller slit, and a 0.2 mm exit slit. Sample rotation was set at 15 rpm. A LynxEye silicon strip position sensitive detector was set with an opening of 3°; the LynxIris was set at 6.5 mm. Data collection was between 2° and 55° 2θ in reflection and between 4° and 55° 2θ in transmission mode, with a step size of 0.02° 2θ and a counting time of 0.3 s per step; with 176 active channels in the detector, this is equivalent to a total counting time of 52.8 s per step.

Rietveld refinements were performed using TOPAS V4.2 (Bruker). Crystal structures were retrieved from the Cambridge Crystal Structure Database: CBZ pure form III CSD code CBMZPNO1;[20] CBZ−SCH form I CSD code UNEZAO.[21] The March−Dollase model for preferred orientation was used on plane (001) for CBZ pure form III and CBZ−SCH form I. The background was modeled with a Chebychev function with five coefficients. All peak shapes were modeled using fundamental parameters based on the geometry of the D8.

Real-time NIR Monitoring. Diffuse reflectance near-infrared (NIR) spectroscopy was continuously performed in-line and noninvasively during hot melt extrusion using an Antaris MX Fourier transform NIR spectrometer (Thermo Scientific, UK). A fiber optic NIR probe was fitted in three different zones of the extruder barrel for in-line monitoring. Spectra were collected in the 10000−4000 cm^{-1} region with a resolution of 16 cm^{-1}. Each spectrum taken was an average of 32 individual scans, which took around 30 s to complete. In addition to real-time monitoring, the extruded cocrystal spectra were measured off-line. Off-line NIR spectra were also collected for the bulk carbamazepine, bulk SCH, and physical mixture of both. Data analysis was performed with the RESULT software (version 3.0, Thermo Scientific, U.K.).

In Vitro Dissolution Study. The in vitro study was conducted on Varian 705 DS dissolution paddle apparatus (Varian Inc., North Carolina, US). Extruded granules, prototype, bulk CBZ, and PM amounts equal to 200 mg of CBZ were placed in 900 mL of 0.1 M hydrochloric acid solution with 37 ± 2 °C set bath temperature at 100 rpm for 2 h. The same studies were carried out in phosphate buffer at pH 6.8. Samples were collected and filtered at predetermined time intervals. Furthermore, the GraphPad Instat (GraphPad Software Inc.) was applied to assist the analysis of the dissolution profiles between the cocrystals and the bulk drug, respectively.

HPLC Analysis. The content of CBZ in all samples was confirmed by HPLC. The experiment was performed on an HPLC system (Aligent Technologies, 1200 series) equipped with a quaternary pump. The mobile phase was 70:30 methanol/water. The sample volume was 20 μL injected by autosampler and scanned at 285 nm using 0.9 mL/min flow rate. A Hypersil 200 mm × 4.6 μm × 5 μm BDS C18 column was employed. Column temperature and retention time were set at 40 °C and 4 min, respectively.

Particle Size Analysis and Morphology. Morphology of all samples including pure CBZ and SCH was examined by SEM (scanning electron microscopy; Hitachi SU8030, Japan). Samples were placed on an aluminum stub and coated with a thin layer of chromium in an argon atmosphere at room temperature. The accelerating voltage of the electron beam was 10 kV to get the SEM images.

The particle size distribution was measured by laser diffraction (Mastersizer 2000, Malvern, U.K.) where 5 g of powders was placed in the dry powder feeder. Sampling time was set at 15 s, and each sample was measured three times.

Stability Studies. The extruded samples and the prototype were placed at controlled room temperature (25 ± 1 °C; 60% ± 1.5% RH) and accelerated (40 ± 1 °C; 75% ± 1.5% RH) conditions, as per ICH guidelines,[22] in a ICH-compliant climatic chamber (Binder KBF 720, SciQuip LTD, U.K.) for a period of 2 weeks.

Molecular Modeling. The ACD/ChemSketch 11.01 and the ACD/3DViewer 11.01 (Ontario, Canada) were used to design the intermolecular interactions between CBZ and SCH cocrystals.

RESULTS AND DISCUSSSION

Hot Melt Extrusion Continuous Processing. In this study, HME, a continuous manufacturing process, was explored for the

dx.doi.org/10.1021/cg401375a | Cryst. Growth Des. 2014, 14, 189−198

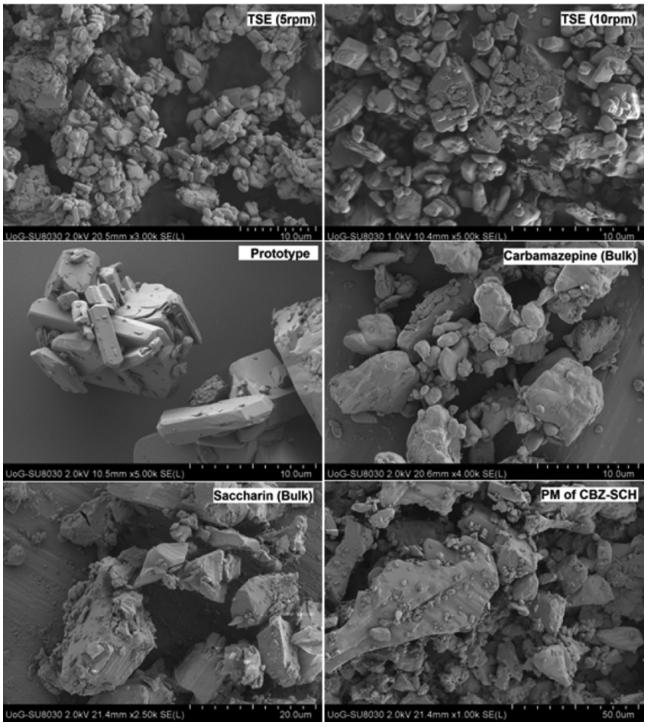

Figure 1. SEM images of bulk CBZ, bulk SCH, physical mixture, CBZ–SCH prototype cocrystals, and extruded TSE (5 and 10 rpm) cocrystals.

development of cocrystals by coprocessing CBZ/SCH blends at a 1:1 molar ratio. The cocrystals were optimized by using single screw (SSE) and twin screw (TSE) extrusion in parallel because processing parameters play a key role in the quality of the obtained materials. The screw type, configuration, and temperature profile were the critical processing parameters (CPP) as previously reported.[17] The solvent method was employed to produce high quality cocrystals, which were used as the prototype for comparison with the HME products.

Initially HME cocrystals were developed with SSE at three different temperatures (120, 135, and 140 °C) in order to identify the optimal extrusion temperature. It was found that 135 °C provided stable and high crystallinity cocrystals. Based on these results, TSE was further employed to improve the cocrystallization process. In both SSE and TSE studies, the die was removed from the extruder because the extrudates were not produced in the form of strands or melted material but rather as granular powder. CBZ decomposed when extrusion temperatures above 145 °C were used (data not shown).

The morphology of the bulk materials, the prototype, and the extrudates was observed with SEM as shown in Figure 1. The crystal shape of bulk CBZ was micronized, flaky, or thin plate-like, whereas the crystals obtained from the solvent process were polyhedral prismatic. These observations are in agreement to previously published studies.[23] In contrast, the shape of the extruded cocrystals was block-shaped. The change of the shape can be explained by the interaction between CBZ and SCH molecules, which results in the modification of the CBZ crystal faces and hence the crystal morphology. However, the influence of the processing parameters should be also considered, and further experimentation is required.

Thermal Analysis. CBZ exhibits enantiotropic polymorphism, which means a transition temperature is observed below the melting point of either of the polymorphs at which both these forms have the same free energy. Above the transition temperature, the higher melting form (I) has the lower free energy and is more stable. In contrast, the lower melting form III is more stable below the transition temperature since it has the lower free energy. The transition temperature of CBZ enantiotropic forms has been reported[24] to be around 71 °C and thus at ambient conditions form III is the most stable. In previous studies,[25] the DSC thermograms of CBZ samples presented two endotherms with the first endotherm between 155 and 165 °C (not followed by any exothermic event), while a sharp endotherm appears between 189 and 192 °C. This small endothermic peak is characteristic of the transition of the anhydrous monoclinic b-form (form III) to the polymorph I and occurs by solid–solid transformation.

The thermophysical properties of the bulk powders, the prototype, and the extruded materials were analyzed using DSC as shown in Figure 2. The thermograms of bulk CBZ showed a melting endothermic peak at 175.31 °C, followed by a second one at 191.50 °C. The bulk SCH thermogram showed a sharp melting peak at 227 °C. In the physical mixture of CBZ–SCH, a shift of the CBZ endothermic peaks at 155.65 and 173.56 °C was observed, while the SCH endotherm was not observed. According to Enxian et al.,[26] the melting endotherm at 155 °C is attributed to the eutectic melt followed by cocrystal melting at 173.56 °C, which is close to the melting endotherm of the produced cocrystals.

In contrast, for the SSE samples, only a single melting endotherm was observed, which varied according to the extrusion temperature as shown in Figure 2a. The endothermic peaks ranged from 168.5 to 171.63 °C, which is below the melting endotherm of the bulk CBZ. All of the SSE endotherms appeared slightly broad with varying melting enthalpy values (ΔH).

The comparison of the melting endotherms revealed that the optimal SSE processing occurred at 135 °C. At this temperature, a narrow melting endotherm with high ΔH was obtained. Powder blends extruded with the twin-screw extruder at low screw speed (5 rpm) presented a single melting endotherm at 174.02 °C ($\Delta H = -107.89$ J/g).

Similarly the extruded blends at higher screw speed (10 rpm) showed a single melting peak at 174.76 °C ($\Delta H = -119.80$ J/g) as shown in Figure 2b. Interestingly, for both TSE screw speeds, the melting endotherms were shifted closer to the prototype's endotherm indicating a more effective mixing process compared with the SSE. In addition, for TSE an increase of the melting enthalpy and narrow melting peaks were observed. The suppression of the CBZ–SCH melting points and the presence of a single melting endotherm suggest the formation of a new entity with a new structure. It is also a strong indication that HME processing facilitates a strong interaction between the CBZ–SCH components, possibly between their functional groups.

In addition, the DSC thermogram of the prototype produced by the solvent process showed a slightly higher sharp melting peak at 177 °C ($\Delta H = -144.91$ J/g). As can be seen in Table 1, higher melting endothermic peaks for the produced cocrystals were combined with higher ΔH values. This suggests a higher purity and crystallinity for the CBZ–SCH prototype and the presence of a low amorphous fraction for the extruded cocrystals.

As shown in Figure 3, HSM was used to further investigate the thermal events of bulk CBZ and the optimized cocrystals. The bulk CBZ showed the formation of needle shaped crystals after melting at 175 °C (form I) followed by a complete melting at 191.7 °C, in good agreement with the DSC thermograms. For

dx.doi.org/10.1021/cg401375a | Cryst. Growth Des. 2014, 14, 189–198

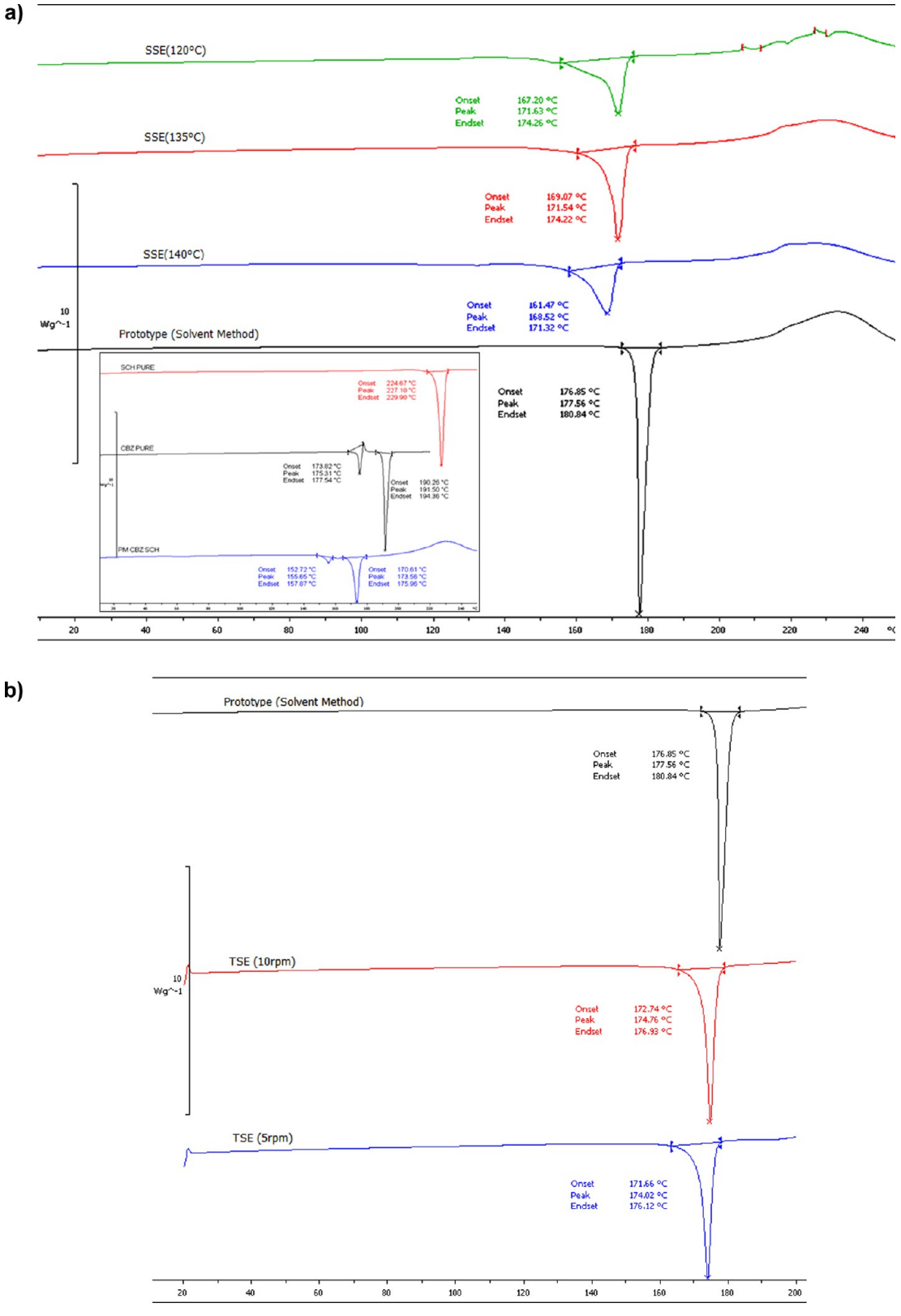

Figure 2. DSC thermograms of (a) cocrystals processed with SSE (120 °C), SSE (135 °C), and SSE (140 °C) and prototype (bulk CBZ, bulk SCH, and physical mixture (PM) in the inset) and (b) CBZ−SCH prototype and CBZ−SCH cocrystals processed with TSE (5 rpm) and TSE (10 rpm).

the prototype, cocrystals could still be observed at 177.5 °C with complete melting at 191.7 °C similar to the pure CBZ. The absence of SCH crystals confirmed the presence of the new entity produced by the solvent approach. The TSE samples showed complete melting of the crystals at 174 and 174.7 °C, respectively. These results confirmed the DSC studies, and only single melting events were observed for both HME and solvent method samples.

dx.doi.org/10.1021/cg401375a | *Cryst. Growth Des.* 2014, 14, 189−198

Table 1. Melting Endothermic Peaks and Normalized Energy of the Bulk, Extruded, and Prototype Substances

substance	peak endotherm (°C)	normalized heat enthalpy (ΔH, J/g)
CBZ bulk (1st peak)	175.31	−28.29
CBZ bulk (2nd peak)	191.50	−102.5
SSE 120 °C	171.63	−76.39
SSE 135 °C	171.54	−85.49
SSE 140 °C	168.52	−71.24
TSE 135 °C (5 rpm)	174.02	−107.89
TSE 135 °C (10 rpm)	174.76	−119.80
prototype	177.56	−144.91

Powder X-ray Diffraction (PXRD). Samples were further analyzed by PXRD to identify the diffraction patterns of the cocrystals formatted by HME and chemical processing. As shown in Figure 4a, the intensity peaks[27,28] of CBZ form III appear at 13.07°, 15.31°, 19.49°, 24.96°, and 27.24° 2θ, while those of bulk SCH appear at 9.56°, 16.02°, 19.13°, and 25.14° 2θ values. In contrast, the diffraction peaks of the CBZ−SCH prototype (Figure 4b) appear at 7.03°, 13.67°, 14.02°, 14.95°, 20.14°, 21.45°, 21.74°, 23.43°, 25.79°, and 28.29° 2θ values, and as it can be seen, they are completely different than those of the individual bulk substances.

Interestingly, the diffraction peaks of both extruded cocrystals, irrespective of the extruder's screw rate, appear to be identical to those of the prototype. However, the characteristic intensity

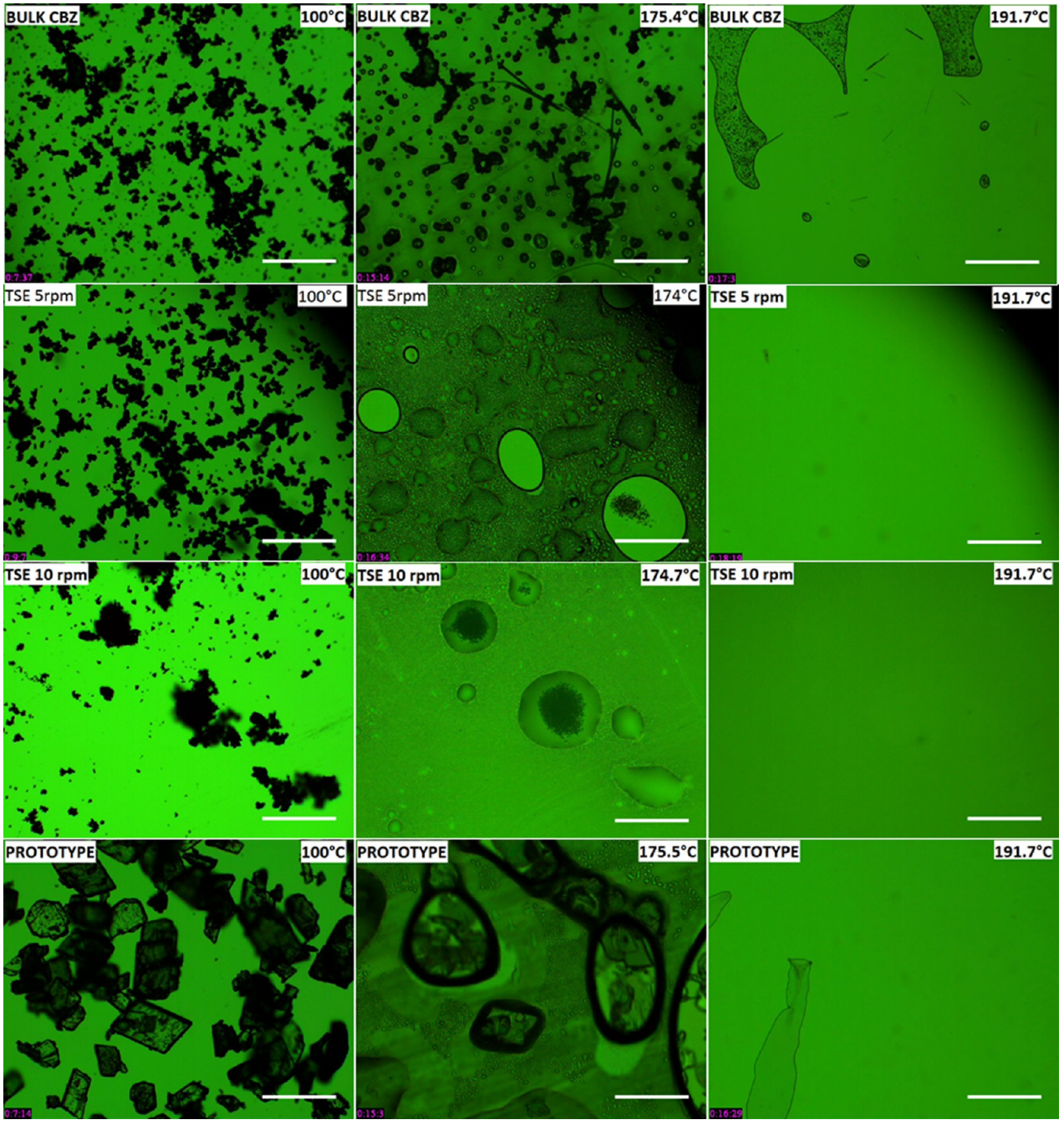

Figure 3. HSM images of bulk CBZ, prototype CBZ−SCH, TSE (5 rpm), and TSE (10 rpm) cocrystals (bar = 200 μm).

dx.doi.org/10.1021/cg401375a | *Cryst. Growth Des.* 2014, 14, 189−198

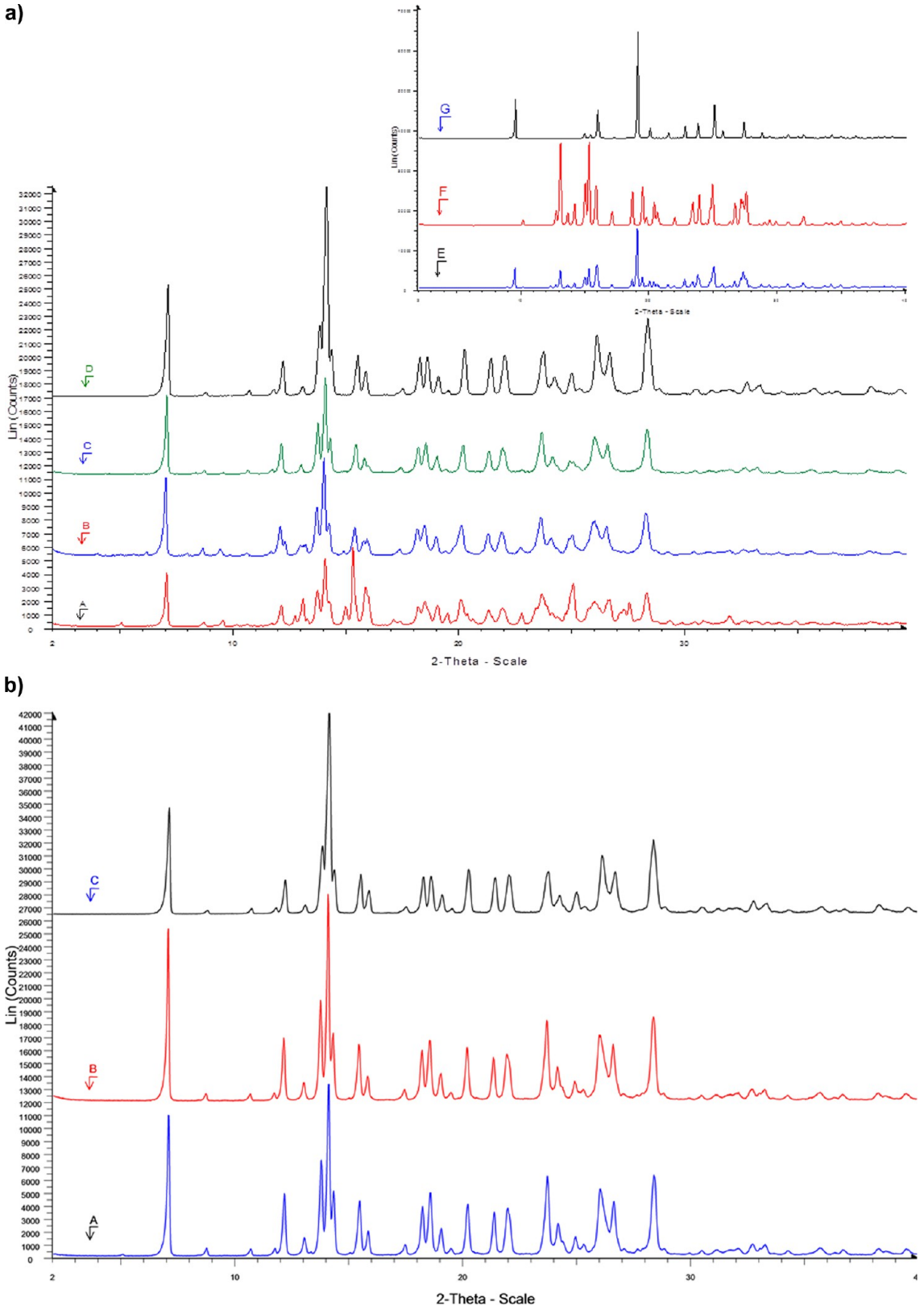

Figure 4. X-ray diffractograms of (a) cocrystals processed with (A) SSE (120 °C), (B) SSE (135 °C), (C) SSE (140 °C), and (D) prototype (in the inset, (E) physical mixture, (F) bulk CBZ, and (G) bulk SCH) and (b) cocrystals processed at (A) TSE (5 rpm), (B) TSE (10 rpm) and (C) prototype.

peaks of the extrudates are lower, indicating a smaller percentage of crystallinity compared with the prototype. This is in agreement with the observed DSC results where a small fraction of amorphous material was identified.

The samples of bulk CBZ (form III) and the two TSE samples of cocrystals CBZ−SCH at the operating conditions of 135 °C and screw speeds of 5 and 10 rpm were analyzed in reflection mode. However, the sample of the prototype demonstrated

dx.doi.org/10.1021/cg401375a | *Cryst. Growth Des.* 2014, 14, 189−198

Table 2. Weight Percent Values for the Calculation of Amorphous Component

		Rietveld	spiked[a]	original[a]
CBZ bulk	amorphous	0	0.55(0.32)	0.92(0.54)
	CBZ-III	59.78	59.45	99.08
	corundum	40.22	40	0
CBZ−SCH (5 rpm)	amorphous	0	1.52(0.36)	2.53(0.61)
	CBZ-SAC-I	59.38	58.48	97.47
	corundum	40.62	40	0
CBZ−SCH (10 rpm)	amorphous	0	1.49(0.5)	2.48(0.8)
	CBZ-SAC-I	59.4	58.51	97.52
	corundum	40.6	40	0
CBZ−SCH (solvent)	amorphous	0	0.02(0.51)	0.04(0.86)
	CBZ-SAC-I	59.99	59.98	99.96
	corundum	40.01	40	0

[a]Error in parentheses.

significant preferred orientation such that a good refinement was not possible in reflection mode. This was subsequently run in transmission mode in Mylar foil, where preferred orientation was reduced and a better fit obtained. In this case, the use of spherical harmonics in the Rietveld refinement further reduced the effect of preferred orientation and lowered the Rwp value to 9.4%.

In Rietveld analysis, the total weight fractions of all the included crystalline phases sum to 1, and the quantity of the amorphous component is not known. However, it can be estimated by using an internal standard addition of a known crystal structure, in this case, a corundum spike. If a significant proportion of amorphous material is present in the sample, then the amount of the spike standard will be overestimated in the normalized Rietveld result since the amorphous component is not measured. TOPAS[29] will calculate the amorphous percentage if the weight fraction of the added spike is known (W_S), since it measures the normalized weight fraction of spike in the Rietveld refinement (R_S). The amorphous percentage (A) is then calculated from the weight fractions:

$$A\% = \frac{(R_S - W_S)}{R_S(1 - W_S)} \times 100 \quad (1)$$

The estimated values for bulk CBZ, prototype, and two TSE cocrystals are depicted in Table 2. As can be seen, the prototype presented very high crystallinity (99.96%) compared with the TSE cocrystals with 97.47% and 97.52%. Interestingly the there

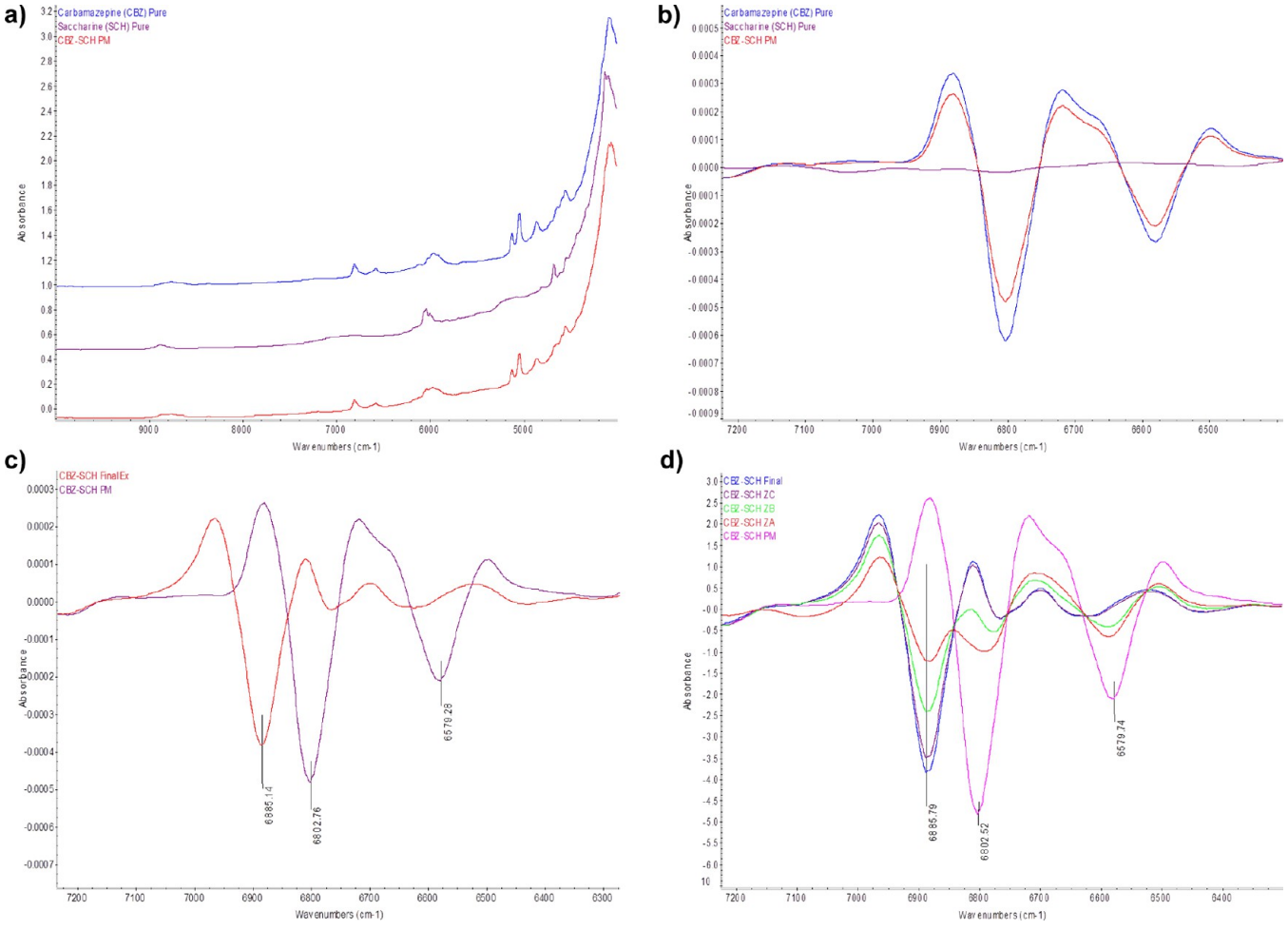

Figure 5. (a) NIR spectra of CBZ (bulk), SCH, and CBZ−SCH physical mixture. (b) Second derivative NIR spectra of CBZ (bulk), SCH, and CBZ−SCH physical mixture in the region of 6400−7100 cm^{-1}. (c) Second derivative spectra of CBZ−SCH PM and the extruded cocrystals (TSE, 5 rpm) in the region between 6400 and 7100 cm^{-1}. (d) Second derivative of in-line NIR spectra in the mixing zones (A, B, C), the TSE (5 rpm) extrudates, and the physical mixture. Each scan is the average of three different batches.

dx.doi.org/10.1021/cg401375a | *Cryst. Growth Des.* 2014, 14, 189−198

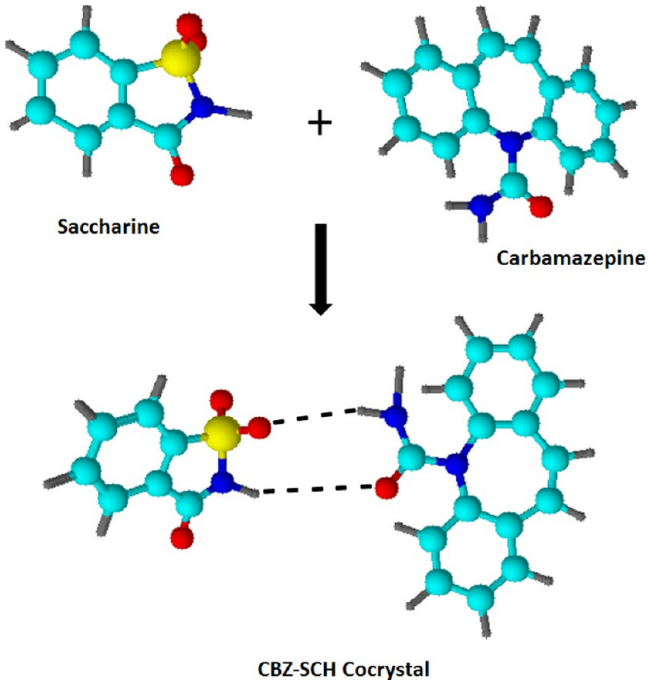

Figure 6. Molecular modeling (3d) of the developed CBZ−SCH form I cocrystals depicting the H-bonding between the functional groups.

was no significant difference between the TSE samples, although slower screw speed showed slightly better results.

The difference between the prototype and the TSE CBZ−SCH cocrystals was attributed to the optimized solvent process compared with the continuous extrusion processing, which can further developed (e.g., altering screw configuration).

Real-Time NIR Monitoring. Off-line NIR spectra of CBZ, SCH, and the physical mixture (PM) were measured to identify the characteristic peaks attributed to the cocrystal. From Figure 5a, it can be easily seen that the NIR spectra of CBZ and SCH present characteristic peaks at different wavelengths.

The spectrum of the PM is represented by the combined spectra of the bulk materials. The second derivative NIR spectra of the PM, CBZ, and the coformer in the 6400−7100 cm^{-1} region are shown in Figure 5b. The spectrum of SCH is almost flat where those of CBZ and the PM are identical and only the peak intensities are different.

Figure 5c depicts the second derivative spectra of the PM and the extruded cocrystals, which show significant differences due to peak shifts. The peak observed at 6579 cm^{-1} could be due to the N−H stretching first overtone of CBZ which has an intramolecular H-bond between =O and N−H of CBZ. This peak reduced as external H-bond formation occurred during extrusion and cocrystallization increased. Another peak at 6802 cm^{-1} was due to the N−H stretching first overtone. This was observed shifted to 6885 cm^{-1} as the H-bond formed between CBZ and SCH. The new peak became more intense as cocrystallization increased. The peak shifting at lower wavenumbers could be attributed to the formation of hydrogen bonding as a result of the formation of cocrystals between CBZ and SCH.[30]

As the CBZ−SCH blends are transferred within the conveying and mixing zones, the formation of cocrystals is expected to gradually take place along the barrel. In order to study further the cocrystal formation, the NIR probe was carefully placed in the three mixing zones, and in-line scans were collected.[31] Figure 5d shows the second derivative spectra of the three different mixing zones and the final extruded cocrystals in comparison to the PM.

It is obvious that the formation of CBZ−SCH cocrystals starts in the first mixing zone and a peak appears at 6885.15 cm^{-1}. The spectra obtained for zones B and C show an increase in the new peak as the extrudate moves toward the end of the extruder. The off-line scan of the final extruded CBZ−SCH cocrystals presents the highest intensity suggesting the completion of the process. These findings suggest that cocrystals were formed gradually due to the increasing mixing capacity across the three mixing zones.

A schematic representation of the H-bonding between the CBZ and SCH molecules is depicted in Figure 6. The X-ray diffractograms are in agreement with the Porter et al.[30] findings where the characteristic intensity peak at 6.9° 2θ is related to the CBZ−SCH form I cocrystals. In this instance, the SCH N−H forms a H-bond with the CBZ carboxyl group, while the CBZ amine group forms a H-bond with the S=O of SCH.[28]

In Vitro Dissolution Study. The in vitro dissolution rate of the produced cocrystals was one of the main criteria to assess their performance. For this reason the dissolution patterns of all extrudates were compared with those of the bulk CBZ and the prototype.

As expected, the bulk CBZ showed a slow dissolution rate with approximately 60% of the drug being dissolved after 2 h (Figure 7a). The CBZ dissolution rate in the PM also showed a low dissolution profile similar to bulk substance without any significant difference suggesting that SCH does not affect the drug dissolution rates. The cocrystal extrudates processed by SSE demonstrated faster dissolution rates depending on the extrusion temperature, increasing in the order 135 °C > 120 °C > 140 °C. The $SSE_{135°C}$ extrudate showed a rapid dissolution rate with 76% of CBZ being dissolved in 30 min, while almost 100% was dissolved in 120 min. Increased dissolution rates were also observed for the $SSE_{120°C}$ extrudate compared with the bulk CBZ (60% in 30 min).

For the $SSE_{140°C}$ extrudate, the CBZ dissolution was slightly higher than the bulk substance due to the low quality of the cocrystals (increased amorphous content). It is obvious that the quality of cocrystals affected their dissolution behavior and confirmed that the optimized $SSE_{135°C}$ cocrystals were of the best quality.

A Kruskal−Wallis nonparametric test followed by the Dunn post hoc multiple comparison test was used to investigate the differences between the three dissolution profiles. This showed a significant difference ($p < 0.05$) for the CBZ cocrystals processed at 120 or 135 °C but not for those at 140 °C.

As shown in Figure 7b, the TSE processed cocrystals also gave increased dissolution rates compared with the prototype. For the $TSE_{(5rpm)}$ extrudate, 61% of CBZ dissolved in 30 min. Interestingly, the CBZ−SCH cocrystals processed at 10 rpm showed slower dissolution (41% in 30 min), suggesting that the screw rate is a critical process parameter.[28] The dissolution performance of the CBZ−SCH prototype was also a key element of this study, and it was compared with those of the extruded cocrystals. Figure 7b shows clearly that the dissolution rate was faster than the bulk substance with 38% dissolving in 30 min and 66% after 60 min. However, the prototype showed significantly lower dissolution rates in comparison to the SSE and TSE processed cocrystals.

In Table 3, the particle size distribution is depicted where the $d[v, 0.5]$ and $d[v, 0.9]$ are recorded for the bulk CBZ, the prototype, and the extruded formulations. The results showed smaller particle size distribution for bulk CBZ but quite larger

dx.doi.org/10.1021/cg401375a | Cryst. Growth Des. 2014, 14, 189−198

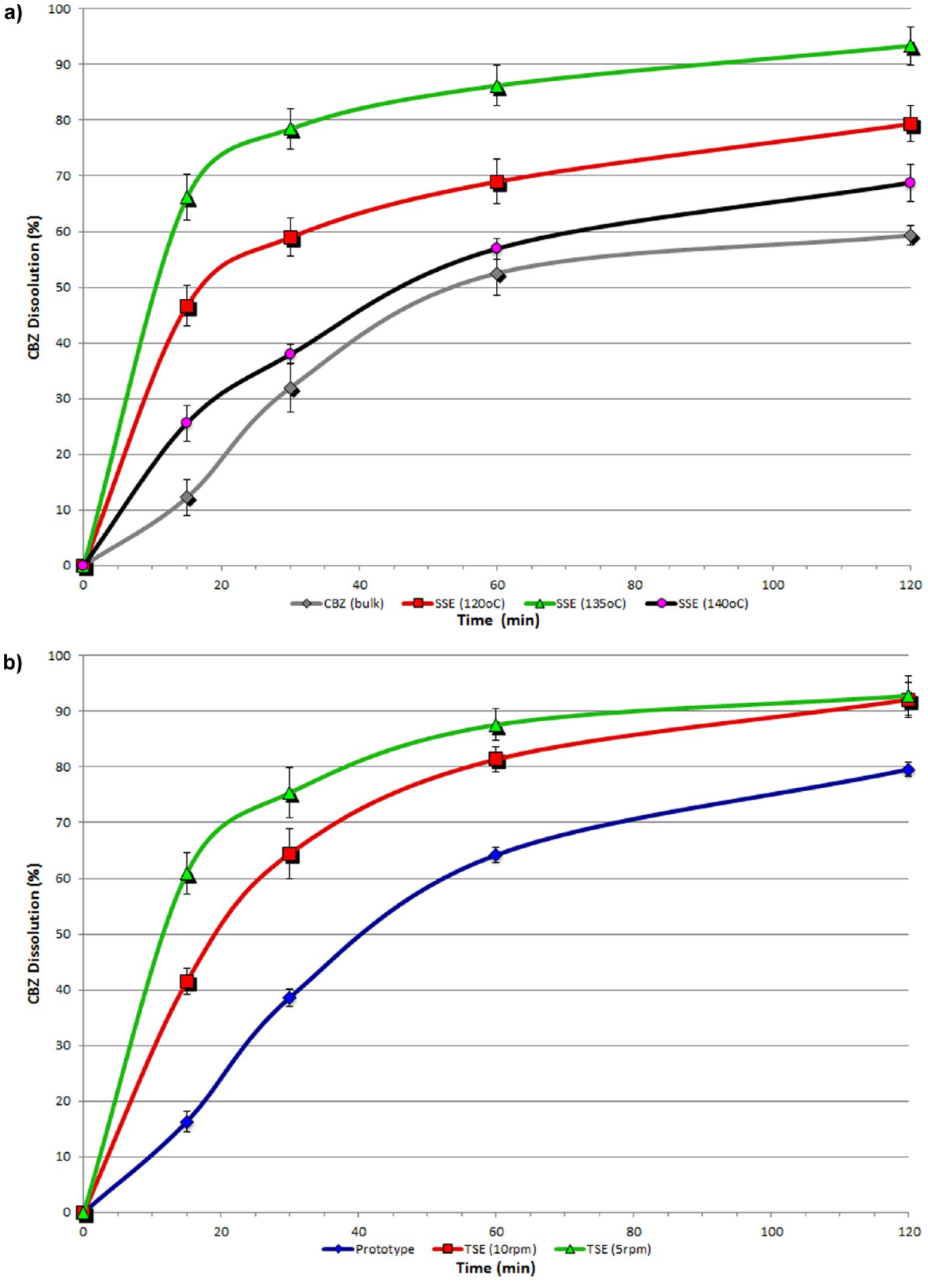

Figure 7. Dissolution profiles (0.1 N HCl, pH 1.2) of (a) bulk CBZ, physical mixture (PM), and CBZ–SCH cocrystals processed with SSE (120 °C), SSE (135 °C), and SSE (140 °C) and (b) CBZ–SCH prototype (MeOH, EtOH solvents) and CBZ–SCH cocrystals processed with TSE (5 rpm) and TSE (10 rpm).

particles for the prototype and the extruded batches. It is obvious that the particle size distribution of the extrudates and the prototype does not favor the dissolution rates of CBZ cocrystals, and thus their faster dissolution rates cannot be attributed to the particle size. Finally, as shown in X-ray analysis the prototype presents higher crystallinity (~2.5%) compared with the TSE batches, and a small amorphous content could affect the dissolution rates. However, it is unlikely that such a small

dx.doi.org/10.1021/cg401375a | *Cryst. Growth Des.* 2014, 14, 189–198

Table 3. Particle Size Analysis of Bulk CBZ, Prototype, and Extrudates by Laser Diffraction

batches	$d[v, 0.5]$ (μm)	$d[v, 0.9]$ (μm)
CBZ bulk	48.31	88.59
SSE	114.65	433.76
$TSE_{(5rpm)}$	105.73	481.69
$TSE_{(10rpm)}$	103.79	369.80
prototype	122.18	419.47

amorphous trace would result in significant increase in the dissolution rates as shown in Figure 7b. In addition, the SSE batches at 120 and 135 °C (Figure 7a) showed slow dissolution rates suggesting that only high purity cocrystals can provide increased dissolution rates.

The dissolution studies were carried out also at pH 6.8, and the same patterns were observed (Supporting Information), only this time the CBZ showed slower dissolution rates in comparison to the acidic media after 2 h.

Stability studies of the produced HME cocrystals (both SSE and TSE) at accelerated conditions (40 °C and 75% RH) showed excellent stability without any changes in the crystallinity. Further X-ray analysis provided identical diffraction peaks without the appearance of any new peaks. These finding were also in a good agreement with similar studies conducted by Hickey et al.[19]

CONCLUSIONS

In conclusion, hot melt extrusion, a continuous manufacturing process, was employed to produce high quality CBZ−SCH cocrystals. The study revealed that extrusion temperature, screw speed, and screw configuration (single or twin screw) were critical processing parameters for the manufacture of high quality cocrystals. The extruded CBZ−SCH cocrystals compared with a CBZ−SCH prototype proved to be of similar quality (high crystallinity) but with faster dissolution rates. In-line NIR investigations showed that cocrystallization took place gradually along the three mixing zones, and optimized cocrystals were obtained at the end of the extrusion processing. Continuous cocrystallization has been shown to be a novel approach for the production of pharmaceutical cocrystals of water insoluble drugs with enhanced performance compared with conventional methods.

ASSOCIATED CONTENT

Supporting Information

Additional dissolution profiles of bulk materials and SSE and TSE extrudates in phosphate buffer (pH 6.8) and X-ray diffraction analysis of extrudates after 2 weeks in accelerated conditions (40 °C and 75% RH). This material is available free of charge via the Internet at http://pubs.acs.org.

AUTHOR INFORMATION

Corresponding Author

*E-mail: D.Douroumis@gre.ac.uk.

Notes

The authors declare no competing financial interest.

REFERENCES

(1) O'Donnell, K.; Williams, R., III. Optimizing the Formulation of Poorly Water-Soluble Drugs. In *Formulating Poorly Water Soluble Drugs*; Williams, R. O., III, Watts, A. B., Miller, D. A., Eds.; Springer: New York: 2012; Vol. 3, pp 27−93.

(2) Good, D. J.; Rodríguez-Hornedo, N. *Cryst. Growth Des.* **2009**, *9* (5), 2252−2264.

(3) Alhalaweh, A.; Velaga, S. P. *Cryst. Growth Des.* **2010**, *10* (8), 3302−3305.

(4) Sanphui, P.; Goud, N. R.; Khandavilli, U. B. R.; Nangia, A. *Cryst. Growth Des.* **2011**, *11* (9), 4135−4145.

(5) Alhalaweh, A.; Sokolowski, A.; Rodríguez-Hornedo, N.; Velaga, S. P. *Cryst. Growth Des.* **2011**, *11* (9), 3923−3929.

(6) De Melo, A. C. C.; De Amorim, I. F.; Cirqueira, M. d. L.; Martins, F. T. *Cryst. Growth Des.* **2013**, *13* (4), 1558−1569.

(7) Schultheiss, N.; Newman, A. *Cryst. Growth Des.* **2009**, *9* (6), 2950−2967.

(8) Friscic, T.; Jones, W. *Faraday Discuss.* **2007**, *136*, 167−178.

(9) Almarsson, O.; Zaworotko, M. J. *Chem. Commun.* **2004**, *40* (17), 1889−1896.

(10) Karki, S.; Friščić, T.; Fábián, L.; Laity, P. R.; Day, G. M.; Jones, W. *Adv. Mater.* **2009**, *21* (38−39), 3905−3909.

(11) Chattoraj, S.; Shi, L.; Sun, C. C. *CrystEngComm* **2010**, *12* (8), 2466−2472.

(12) Miroshnyk, I.; Mirza, S.; Sandler, N. *Expert Opin. Drug Delivery* **2009**, *6* (4), 333−341.

(13) Vishweshwar, P.; McMahon, J. A.; Bis, J. A.; Zaworotko, M. J. *J. Pharm. Sci.* **2006**, *95* (3), 499−516.

(14) Yadav, A. V.; Shete, A. S.; Dabke, A. P.; Kulkarni, P. V.; Sakhare, S. S. *Indian J. Pharm. Sci.* **2009**, *71* (4), 359−70.

(15) Buanz, A. B. M.; Telford, R.; Scowen, I. J.; Gaisford, S. *CrystEngComm* **2013**, *15* (6), 1031−1035.

(16) Andrews, G. P.; Jones, D. S.; Diak, O. D.; Margetson, D. M.; McAllister, M. S. *Pharm. Technol. Eur.* **2009**, *21* (1), 24−27.

(17) Dhumal, R.; Kelly, A.; York, P.; Coates, P.; Paradkar, A. *Pharm. Res.* **2010**, *27* (12), 2725−2733.

(18) Daurio, D.; Medina, C.; Saw, R.; Nagapudi, K.; Alvarez-Núñez, F. *Pharmaceutics* **2011**, *3* (3), 582−600.

(19) Hickey, M. B.; Peterson, M. L.; Scoppettuolo, L. A.; Morrisette, S. L.; Vetter, A.; Guzmán, H.; Remenar, J. F.; Zhang, Z.; Tawa, M. D.; Haley, S.; Zaworotko, M. J.; Almarsson, Ö. *Eur. J. Pharm. Sci.* **2007**, *67* (1), 112−119.

(20) Reboul, J. P.; Cristau, B.; Soyfer, J. C.; Astier, J. P. *Acta Crystallogr., Sect. B: Struct. Sci.* **1981**, *37* (10), 1844−1848.

(21) Fleischman, S. G.; Kuduva, S. S.; McMahon, J. A.; Moulton, B.; Bailey Walsh, R. D.; Rodríguez-Hornedo, N.; Zaworotko, M. J. *Cryst. Growth Des.* **2003**, *3* (6), 909−919.

(22) ICH: Q1A(R2). Stability testing of new drug substances and products (2nd revision). ICH Steering Committee; 2003

(23) Nokhodchi, A.; Bolourtchian, N.; Dinarvand, R. *J. Cryst. Growth* **2005**, *274* (3−4), 573−584.

(24) Behme, R. J.; Brooke, D. *J. Pharm. Sci.* **1991**, *80* (10), 986−990.

(25) Moneghini, M.; Kikic, I.; Voinovich, D.; Perissutti, B.; Filipović-Grčić, J. *Int. J. Pharm.* **2001**, *222* (1), 129−138.

(26) Enxian, L.; Rodriguez-Hornedo, N.; Suryanarayanan, R. *CrystEngComm* **2008**, *10*, 665−668.

(27) Rustichelli, C.; Gamberini, G.; Ferioli, V.; Gamberini, M. C.; Ficarra, R.; Tommasini, S. *J. Pharm. Biomed. Anal.* **2000**, *23* (1), 41−54.

(28) Grzesiak, A. L.; Lang, M.; Kim, K.; Matzger, A. J. *J. Pharm. Sci.* **2003**, *92*, 2260−2271.

(29) De La Torre, A. G.; Bruque, S.; Aranda, M. A. G. J. *Appl. Crystallogr.* **2001**, *34* (2), 196−202.

(30) Porter, W. W., III.; Elie, S. C.; Matzger, A. J. *Cryst. Growth Des.* **2008**, *8* (1), 14−16.

(31) Kelly, A. L.; Gough, T.; Dhumal, R. S.; Halsey, S. A.; Paradkar, A. *Int. J. Pharm.* **2012**, *426* (1−2), 15−20.